Nanocomposite lanthanum strontium manganite thin films formed by using a chemical solution deposition

C. Moreno,[1,a] P. Abellán,[1] F. Sandiumenge,[1] M.-J. Casanove,[2] and X. Obradors[1]

[1]Institut de Ciència de Materials de Barcelona (ICMAB-CSIC), UAB, 08193 Bellaterra, Catalonia, Spain
[2]Centre d'Elaboration des Materiaux et d'Etudes Structurales, CNRS, BP 4347, 29 rue J. Marvig, F-31055 Toulouse Cedex 4, France

A single-step process to prepare epitaxial nanocomposite $La_{0.7}Sr_{0.3}MnO_3/La_2O_3$ thin films formed by spontaneous phase separation using a chemical solution deposition is presented. High magnetic field and temperature dependences of magnetic, transport, and magneto-transport properties of the films were investigated. The relationship between the enhanced magnetoresistance and microstructure and chemical inhomogeneities of the films are discussed. © 2012 American Institute of Physics. [doi:10.1063/1.3675461]

Nanocomposites of colossal magnetoresistance (MR) manganites have recently attracted considerably interest for the possibility of tailoring the magnetotransport properties.[1–3] Most of the reported approaches are based on polycristalline ceramics with granular second phases where the control of the intergrain interface properties is not easy. In contrast, epitaxial nanocomposite films with well ordered phase boundaries are completely different materials where a fine tuning can be achieved.[1,4] Chemical solution deposition (CSD) has been demonstrated to be a cost-effective methodology to grow high quality films.[5,6]

In this work, we present a single-step process to prepare epitaxial nanocomposite $La_{0.7}Sr_{0.3}MnO_3$ (LSMO) thin films grown on (100)-$SrTiO_3$ (STO) substrates by spontaneous phase separation of a secondary La oxide phase.

Stoichiometric LSMO thin films and nanocomposite LSMO thin films with a 20% and 40% excess of La were prepared by metal-organic decomposition as described elsewhere.[7] Their structure was analyzed by x-ray diffraction and transmission electron microscopy (TEM) using a spherical aberration corrected Tecnai F20 electron microscopes at 200 kV fitted with a GIF-Tridiem energy filter. Transport properties were measured properly in lithographed films[8] by the four point technique using a quantum design physical property measurement system and magnetic measurements were carried out with a superconducting quantum interference device (SQUID) magnetometer.

Surface morphologies of the stoichiometric and 20% excess of La LSMO thin films were found to have spontaneous formation of self-assembled insulating nanodots at the film surface.[7] In contrast, the 40% excess of La LSMO thin films display a rough surface structure where the insulating nanodot concentration nearly vanishes, as observed in the scanning force microscopy (SFM) image in Fig. 1(a) and in its corresponding current map, Fig. 1(b), obtained by conducting scanning force microscopy (C-SFM).[9]

Fig. 1(c) displays a low magnification TEM image of the composite film grown with 40% excess of La. Film thickness is in the range of 26-35 nm. Contrast changes suggest that the film is composed of different phases and/or orientations of the same phase which, in any case, makes the structure of the film to be non homogeneous.

In order to investigate chemical homogeneity of the composite films, energy filtered TEM (EFTEM) analysis was performed. Figures 1(e) and 1(f) are La and Mn elemental maps of the area shown in the low magnification TEM image in (d), respectively. As indicated in the region surrounded by a dashed line, there are areas with enriched La and poor Mn contents. Particles with this common characteristic have been found all along the films and their sizes run from a few nanometers to the entire film thickness. These regions should
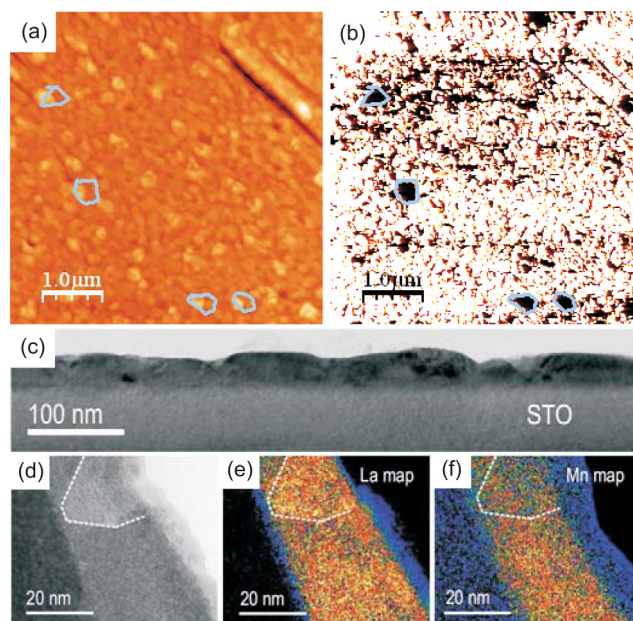

FIG. 1. (Color online) LSMO/STO thin film with 40% excess of La. (a) Topographic SFM image and (b) current map ($V = -2$ V) corresponding to the same surface displayed in (a) where some insulating regions (black regions) are encircled to observe the correspondence of these regions in the topographic image. Current scale from 0 nA (black) to -10 nA (white). (c) Cross-section low magnification TEM image showing the presence of different grains evidenced by the contrast changes in the image. (d) Low magnification TEM image and corresponding La-$M_{5,4}$ edge, (e), and Mn-$L_{3,2}$ edge, (f), filtered images.

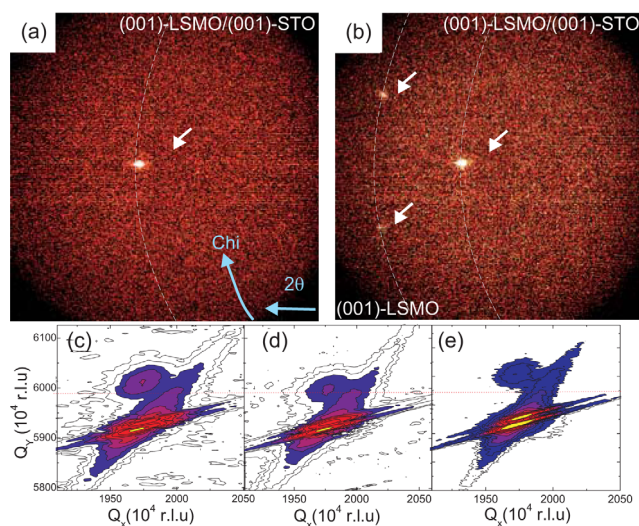[a]Electronic mail: cesar.moreno.sierra@upc.edu.

FIG. 2. (Color online) X-ray diffraction pattern $\theta - 2\theta$ of the LSMO thin films grown on STO with (a) stoichiometric composition and (b) 40% excess of La. The x axis corresponds to 2θ and the vertical parabolic line corresponds to χ which varies with constant 2θ. The Bragg peaks of the (001)-STO and (001)-LSMO phases are identified in addition to the (110)-LSMO reflection. Reciprocal space maps around the (103) reflections of LSMO and STO of the stoichiometric (c), 20% (d), and 40% (e) excess of La films. rlu means "reciprocal lattice units" and 1 rlu $= 2/\lambda$ with $\lambda = 0.154184$ nm.

be most likely correlated with the insulating regions showed in the current map (Fig. 1(b)).

Nevertheless, nanocomposite LSMO films show a high degree of epitaxy confirmed by $\theta - 2\theta$ x-ray diffraction pattern obtained with a general area detector diffraction system (GADDS) equipped with a 2D x-ray detector. Cube-on-cube orientation relationship (001)LSMO//(001)STO was determined for the stoichiometric, Fig. 2(a), and the 40% excess of La, Fig. 2(b), LSMO films. Furthermore, for the nanocomposite with 40% excess of La, two additional discrete (110)LSMO peaks were detected associated to a slight deviation from perpendicularity respect to the substrate. It is worth noting that no ring structures associated to randomly oriented phases were found in the diffraction patterns.

Reciprocal space mapping was performed in order to explore the stress state of the nanocomposites relative to stoichiometric films. The reciprocal space maps of (103) LSMO and STO substrate reflections are shown in Figures 2(c)–2(e) for films with different La excess contents. The in-plane (out-of-plane) parameter for stoichiometric films was determined to be $a = 3.905$ Å ($c = 3.851$ Å) in-plain parameter matches with the substrate $a_{STO} = 3.905$ Å. For the 20% nanocomposite films, it was determined to be $a = 3.898$ Å ($c = 3.855$ Å) and for the 40% nanocomposite ones, it is $a = 3.908$ Å ($c = 3.852$ Å). Thus, the stoichiometric and nanocomposite films are fully strained (expanded biaxial tensile strain) and only a slight relaxation is observed for the 20% La excess sample. These findings are in contrast to thicker fully relaxed ($La_{0.7}Sr_{0.3}MnO_3$-$(Sr,La)O_x$) nanocomposite thin films where $(Sr,La)O_x$ secondary phases contributed to the misfit relaxation of the LSMO nanocomposite films.[10]

An identification of the different phases in the composite films was performed by analysis of high-resolution TEM (HRTEM) images taken at different locations along the films. In Fig. 3(a), HRTEM image of an inclusion embedded
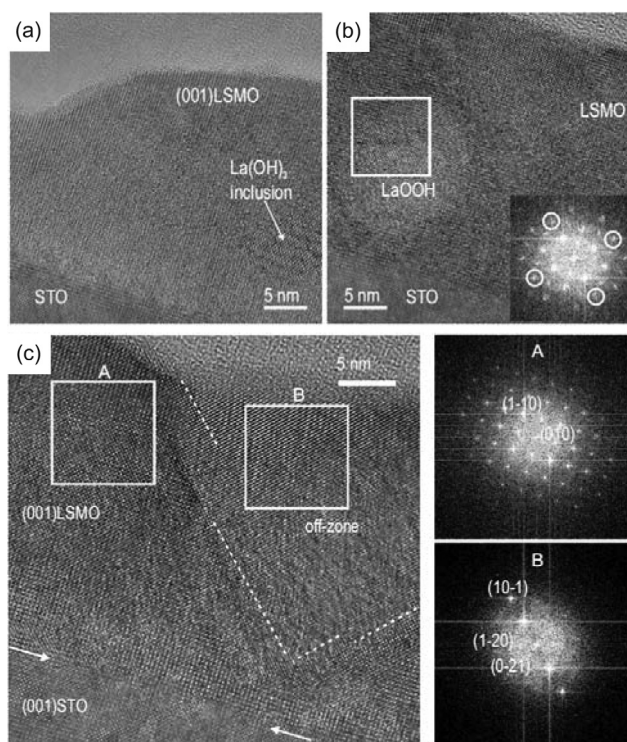

FIG. 3. HRTEM images showing different inclusions with crystal structure consistent with hexagonal $La(OH)_3$ (a) and monoclinic LaO(OH) (b). Cross-section HRTEM image exhibiting a misoriented LSMO grain (FFT in B) with grain thickness being almost that of the epitaxial LSMO film (FFT in A).

in the LSMO film is shown. The corresponding FFT spectrum is consistent with the hexagonal $La(OH)_3$ phase (JCPDS 83-2034). According to previous works, this phase is most likely derived from the hexagonal La_2O_3 phase in air.[11] Also, inclusions exhibiting a FFT spectrum consistent with monoclinic LaO(OH) phase (JCPDS 77-2349), as seen along the [001] and/or [101] zone axis, are observed. In Figure 3(b), one of these inclusions is shown; it presents a high degree of mosaicity and structural disorder. This form of La hydroxide has been reported to be a common product from the cubic La_2O_3 when exposed to air.[11,12] Hence, TEM analysis revealed a massive presence of these two La-O phases. Most likely, hexagonal and cubic La_2O_3 were formed during film synthesis, which reacted with air moisture to form hydroxides when preparing the TEM sample. Besides the large number of La-rich inclusions found in the film, misoriented LSMO grains were also observed. Fig. 3(c) is a HRTEM image showing an off-axis LSMO grain. The interface to the STO substrate is indicated by the white arrows for clarity. The two domains shown in the image are coherent along the (1-10) planes, indicating that this is a common plane to both orientations. Rotation occurs along an axis normal to the (1-10) planes; i.e., along the [1-10] axis. The FFT patterns on the right hand side correspond to the [001] zone axis of the LSMO phase obtained from A and to a misoriented grain near the [212] zone axis in grain B. This latter zone axis is at 48° from the [001] zone axis. From the image features and the FFT pattern, the grain observed in B could be 3°-5° away from that zone axis.

Temperature dependences of magnetization of the films are shown in Fig. 4(a). The magnetic transition for all thin
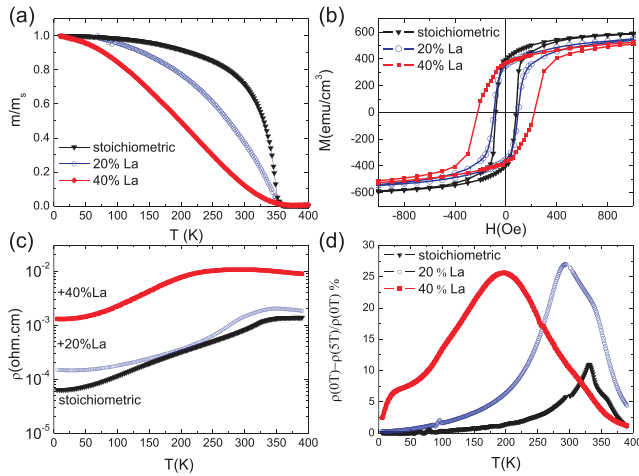
FIG. 4. (Color online) Magnetic and transport properties of the films. (a) Temperature dependence of magnetization taken after field cooling at 0.5 T in-plane applied magnetic field. (b) Isothermal hysteresis magnetic loops at 10 K. (c) Temperature dependence of resistivity at 0 T. (d) Magnetoresistance as a function of temperature measured at 5 T.

films is about 350 K, although for the 20% and 40% nanocomposite films, the magnetic transitions have a reduced sharpness. This finding may be associated with the chemical and structural inhomogeneities observed by EFTEM which promoted a depression of the double exchange mechanism. The films demonstrate ferromagnetic hysteresis at 10 K (Fig. 4(b)). The increase in coercive field for the 40% nanocomposite film put in evidence the role of the misoriented LSMO grains observed by HRTEM as a domain wall pinning centers.

As a result of the presence of the La inclusions and the chemical disorder untangled by EFTEM, an increase of $\approx 2300\%$ in the resistivity at 5 K is observed for the 40% nanocomposite films as compared to stoichiometric thin films (see Fig. 4(c)). At this point, it is important to note that the residual resistivity at 5 K for the stoichiometric film is similar to that previously reported for $La_{0.7}Sr_{0.3}MnO_3$ single crystal films[13] ($<10^{-4}$ Ω cm). Furthermore, the metal-insulator transition temperature, T_{MI} (see Fig. 4(c)) decreases (T_{MI} calculated as the maximum in the differential resistivity $d\rho/dT$ which in our case match with the maximum of the MR at 5 T), while the MR peak broadens and moves to lower temperatures as La excess increases (Fig. 4(d)). In particular, the MR increases by a factor of more than 2 for the 20% and

40% nanocomposite films as compared to the stoichiometric one. Very likely, the increase in resistivity and MR is due to both, the formation of grain boundaries among misoriented grains and the chemical disorder of the nanocomposite.

In summary, a simple approach to create nanocomposite thin films through spontaneous phase separation based on CSD was developed. The La excess content is accommodated by the formation of La-rich inclusions embedded in the epitaxial LSMO thin film matrix. These properties are tuned by La excess content, with enhanced magnetoresistance in a whole range of temperature associated to the existence of misoriented grains of LSMO and the created secondary phases.

[1]A. Chen, Z. Bi, C.-F. Tsai, J. Lee, Q. Su, X. Zhang, Q. Jia, J. L. MacManus-Driscoll, and H. Wang, Adv. funct. Mater. **21**, 2423 (2011).
[2]J. L. MacManus-Driscoll, P. Zerrer, H. Wang, H. Yang, J. Yoon, A. Fouchet, R. Yu, M. G. Blamire, and Q. Jia, Nature Mater. **7**, 314 (2008).
[3]V. Moshnyaga, B. Damaschke, O. Shapoval, A. Belenchuk, J. Faupel, O. I. Lebedev, J. Verbeeck, G. van Tendeloo, M. Mucksch, V. Tsurkan *et al.*, Nature Mater. **2**, 247 (2003).
[4]J. L. MacManus-Driscoll, Adv. funct. Mater. **20**, 2035 (2010).
[5]J. Gutierrez, A. Llordés, J. Gazquez, M. Gibert, N. Roma, S. Ricart, A. Pomar, F. Sandiumenge, N. Mestres, T. Puig *et al.*, Nature Mater. **6**, 367 (2007).
[6]P. Abellán, F. Sandiumenge, M.-J. Casanove, M. Gibert, A. Palau, T. Puig, and X. Obradors, Acta Mater. **59**, 2075 (2011).
[7]C. Moreno, P. Abellán, A. Hassini, A. Ruyter, A. P. del Pino, F. Sandiumenge, M. J. Casanove, J. Santiso, T. Puig, and X. Obradors, Adv. Funct. Mater. **19**, 2139 (2009).
[8]C. Moreno, C. Munuera, A. Pérez del Pino, J. Gutiérrez, T. Puig, C. Ocal, X. Obradors, and A. Ruyter, Phys. Rev. B **80**, 094412 (2009).
[9]C. Moreno, C. Munuera, S. Valencia, F. Kronast, X. Obradors, and C. Ocal, Nano Lett. **10**, 3828 (2010).
[10]P. Abellán, C. Moreno, F. Sandiumenge, X. Obradors, and M.-J. Casanove, Appl. Phys. Lett. **98**, 041903 (2011).
[11]M. Nieminen, M. Putkonen, and L. Niinisto, Appl. Surf. Sci. **174**, 155 (2001).
[12]L. G. Rovira, J. M. Sanchez-Amaya, M. Lopez-Haro, A. B. Hungria, Z. Boukha, S. Bernal, and F. J. Botana, Nanotechnology **19**, 495305 (2008).
[13]A. Urushibara, Y. Moritomo, T. Arima, A. Asamitsu, G. Kido, and Y. Tokura, Phys. Rev. B **51**, 14103 (1995).